

An efficient finite-difference scheme for computation of electron states in free-standing and core-shell quantum wires

V. V. Arsoški^{a,*}, N. A. Čukarić^{a,b}, M. Ž. Tadić^a, F. M. Peeters^b

^a*School of Electrical Engineering, University of Belgrade, P.O. Box 35-54, 11120 Belgrade, Serbia*

^b*Department of Physics, University of Antwerp, Groenenborgerlaan 171, B-2020 Antwerp, Belgium*

Abstract

The electron states in axially symmetric quantum wires are computed by means of the effective-mass Schrödinger equation, which is written in cylindrical coordinates φ , ρ , and z . We show that a direct discretization of the Schrödinger equation by central finite differences leads to a non-symmetric Hamiltonian matrix. Because diagonalization of such matrices is more complex it is advantageous to transform it in a symmetric form. This can be done by the Liouville-like transformation proposed by Rizea et al. (Comp. Phys. Comm. 179 (2008) 466-478), which replaces the wave function $\psi(\rho)$ with the function $F(\rho) = \psi(\rho)\sqrt{\rho}$ and transforms the Hamiltonian accordingly. Even though a symmetric Hamiltonian matrix is produced by this procedure, the computed wave functions are found to be inaccurate near the origin, and the accuracy of the energy levels is not very high. In order to improve on this, we devised a finite-difference scheme which discretizes the Schrödinger equation in the first step, and then applies the Liouville-like transformation to the difference equation. Such a procedure gives a symmetric Hamiltonian matrix, resulting in an accuracy comparable to the one obtained with the finite element method. The superior efficiency of the new finite-difference scheme (*FDM*) is demonstrated for a few ρ -dependent one-dimensional potentials which are usually employed to model the electron states in free-standing and core-shell quantum wires. The new scheme is compared with the other *FDM*

*Corresponding author.

E-mail address: vladimir.arsoski@etf.bg.ac.rs

schemes for solving the effective-mass Schrödinger equation, and is found to deliver energy levels with much smaller numerical error for all the analyzed potentials. It also gives more accurate results than the scheme of Rizea et al., except for the ground state of an infinite rectangular potential in freestanding quantum wires. Moreover, the \mathcal{PT} symmetry is invoked to explain similarities and differences between the considered *FDM* schemes.

Keywords: quantum wire, finite difference, finite element, discretization, eigenvalue, effective-mass

1. Introduction

Recent advances in nanowire (quantum wire) fabrication technology have led to an increased interest in the *vapor-liquid-solid* (VLS) method [1]. It is a bottom-up process, which has been used to produce freestanding quantum wires [2], core-shell quantum wires [3, 4], nanowire superlattices [5], branched nanowires [6], etc. They have been made out of various semiconductors, including III-V compounds [3], silicon [7], germanium [8], and their alloys. The huge progress in the field has been driven by actual and potential applications of nanowires in electronics and photonics. For example, transistors [9], photovoltaic devices [10], light-emitting diodes [11], lithium batteries [12], and chemical and biological sensors [13] have all been realized using nanowires.

In addition to advances in production tools, the models of electronic structure of quantum wires has substantially progressed during time, both in increasing complexity and higher precision [14]. For example, *ab initio* methods are currently able to predict experimental results with sub-meV accuracy [14], but are overcomplex to use for large wires. For the latter, however, use of the effective methods, such as the effective-mass and $\mathbf{k} \cdot \mathbf{p}$ theories, may be suitable [15, 16, 17, 18]. We note that modeling of electronic structure is essentially important to understand transport and optical properties of nanostructures and nanodevices. Moreover, the electronic structure models of quantum wires provide a reliable and an inexpensive way to design quantum wire systems with specific properties.

A convenient model for the electron states in quantum wires which are wider than about 2 nm is the effective-mass theory. It has the form of the Schrödinger equation written for the case of position dependent effective mass, and is able to capture the essential physics of the electron states. In practice it usually assumes that the confinement potential arises from a

band offset between different semiconductors, yet the eigenproblem is usually only numerically solvable. For example, the wave function can be expanded in a basis of analytical functions [19]. But such an approach is known to produce dense Hamiltonian matrices, and could have low accuracy of the wave functions around numerical boundaries [20]. An attractive alternative is the finite-difference method (*FDM*) [21], which employs a discretization of the wave function and its derivatives on a grid [22, 23]. Finite difference approximations are usually of low order [23], therefore the *FDM* delivers sparse matrices which could be diagonalized extremely fast. As a matter of fact, the *FDM* has been adopted to numerically solve various equations in physics [24, 25, 26]. For example, the Poisson equation and the Schrödinger equation are solved together in the Hartree calculation of exciton states by using the same *FDM* discretization [27]. The robustness of the *FDM* has been an essential criterion for its frequent use to model systems where the electrons are confined in more than one dimension, quantum wires and quantum dots [27], for example.

When applying the *FDM* to solve the Schrödinger equation, a grid should be constructed with special care about the regions close to the interfaces. It is not a difficult task when quantum wires have axial symmetry, which allows reducing the eigenproblem to the computation of matrix elements that depend on only the ρ coordinate of the cylindrical system. However, the effective-mass Schrödinger equation contains a term proportional to the first derivative of the wave function with respect to the radius. Because of this term the finite-difference approximation makes the Hamiltonian matrix nonsymmetric.

In this paper, we study how the *FDM* is used to solve the effective-mass Schrödinger equation for axially symmetric potentials that appear in free-standing and core-shell quantum wires. In the case of freestanding quantum wires, an infinite rectangular potential and the potential of a 2D linear harmonic oscillator are analyzed, shown schematically in Figs. 1(a) and (b). Core-shell quantum wires are considered for: (1) the type-Ic potential [17], where the electron is confined inside the core, and (2) the type-Is potential [17], which confines the electron in the shell. Both analyzed potentials in core-shell quantum wires are assumed to have stepwise variation with ρ , which is displayed in Figs. 1(c) and (d). A few discretization *FDM* schemes are constructed to solve the eigenproblem. *First*, the original Schrödinger equation is discretized by central differences, and it is demonstrated that the Hamiltonian matrix is asymmetric. Furthermore, for computing the states of

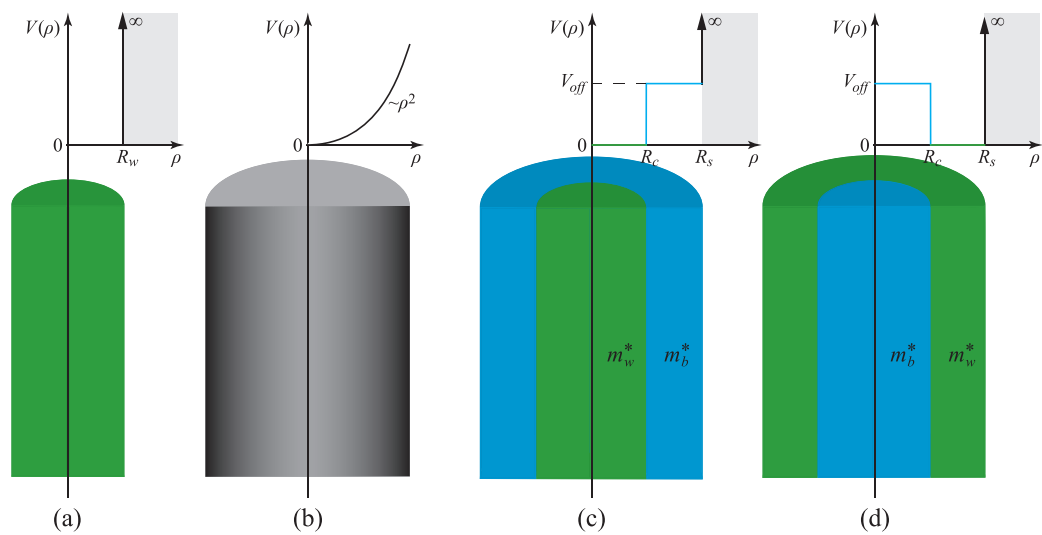


Figure 1: The considered potentials in the analyzed cylindrical quantum wires: (a) the infinite rectangular potential well in a free-standing quantum wire, (b) the potential of a linear harmonic oscillator, (c) the confining potential inside the core of a core-shell quantum wire, and (d) the confining potential inside the shell of a core-shell quantum wire.

zero orbital momentum two types of boundary conditions are tested and compared. *Second*, the Schrödinger equation is transformed into another equation [28] by the Liouville-like (*LL*) transformation, which removes the problematic term from the Hamiltonian. When the *LL*-transformed Schrödinger equation is discretized by the *FDM*, the Hamiltonian matrix becomes symmetric. However, the boundary condition at the inner boundary is such that the wavefunctions are inaccurately computed close to the origin. The *third* method is an approach developed by us, which employs the finite-difference discretization of the original Schrödinger equation, and subsequently applies the Liouville-like transformation to the obtained difference equation. This approach is novel to the best of our knowledge and is able to solve the problem of insufficient accuracy of the solution of the *LL*-transformed Schrödinger equation, and in the same time delivers a symmetric Hamiltonian matrix. The accuracies of the three discretization schemes are mutually compared for the analyzed model potentials, and we compare the results with those from the finite element method (*FEM*).

The paper is organized as follows. In Sec. II the discretization schemes to solve the effective-mass Schrödinger equation for quantum wires are presented. Sec. III contains the error analysis on the example of a constant effective mass in the structure. Sec. IV presents the results of our computations. We conclude in Sec V.

2. The model of the electron states and the FDM schemes

2.1. The model

We compute the electron states by using the effective-mass Schrödinger equation

$$H_{3D}\Psi_{3D}(\mathbf{r}) = E\Psi_{3D}(\mathbf{r}). \quad (1)$$

Here, H_{3D} denotes the single-band effective-mass Hamiltonian,

$$H_{3D} = \frac{1}{2}\mathbf{p}\frac{1}{m^*(\mathbf{r})}\mathbf{p} + V(\mathbf{r}), \quad (2)$$

where $m^*(\mathbf{r})$ is the position dependent electron effective mass, $\mathbf{p} = -i\hbar\nabla$ is the canonical momentum operator, and $V(\mathbf{r})$ is the confining potential of the electron. In an axially symmetric quantum wire grown along the z direction, $V(\mathbf{r}) = V(\rho)$ and $m^*(\mathbf{r}) = m^*(\rho)$, where ρ is the radius in the cylindrical coordinate system. Thus the envelope function has the form

$$\Psi_{3D}(\mathbf{r}) = C e^{ik_z z} \Psi_{2D}(\rho, \varphi), \quad (3)$$

where $C = \text{const}$, φ is the polar angle, and k_z is a good quantum number representing the translational symmetry along the z direction. It reduces the complexity of the eigenproblem to two coordinates, ρ and φ ,

$$H_{2D}\Psi_{2D}(\rho, \varphi) = E\Psi_{2D}(\rho, \varphi), \quad (4)$$

where

$$H_{2D} = -\frac{\hbar^2}{2} \left[\frac{1}{\rho} \frac{\partial}{\partial \rho} \left(\frac{\rho}{m^*} \frac{\partial}{\partial \rho} \right) + \frac{1}{m^*} \frac{1}{\rho^2} \frac{\partial^2}{\partial \varphi^2} \right] + V(\rho). \quad (5)$$

We can furthermore reduce the complexity by invoking the axial symmetry,

$$\Psi_{2D}(\mathbf{r}) = \frac{1}{\sqrt{2\pi}} e^{il\varphi} \psi(\rho), \quad (6)$$

where l denotes the orbital quantum number which represents quantization of the z projection of the electron angular momentum L_z . The Schrödinger equation for ψ is then

$$-\frac{\hbar^2}{2} \left[\frac{1}{\rho} \frac{d}{d\rho} \left(\frac{\rho}{m^*} \frac{d\psi(\rho)}{d\rho} \right) - \frac{l^2\psi(\rho)}{m^*\rho^2} \right] + \left(V(\rho) + \frac{\hbar^2 k_z^2}{2m} \right) \psi(\rho) = E\psi(\rho), \quad (7)$$

which is written compactly as

$$H\psi = E\psi. \quad (8)$$

We will hereafter consider only the case $k_z = 0$, since the computation of the $k_z \neq 0$ states does not bring any qualitative difference to the obtained results. With other words, we model only the states of the quantum wire subband bottoms. Expanding the first term on the left hand side of Eq. (7), the Schrödinger equation for $k_z = 0$ becomes

$$\begin{aligned} & -\frac{\hbar^2}{2} \left[\frac{1}{m^*} \frac{d^2\psi(\rho)}{d\rho^2} + \frac{1}{m^*} \frac{1}{\rho} \frac{d\psi(\rho)}{d\rho} + \frac{d}{d\rho} \left(\frac{1}{m^*} \right) \frac{d\psi(\rho)}{d\rho} - \frac{l^2\psi(\rho)}{m^*\rho^2} \right] \\ & + V(\rho)\psi(\rho) = E\psi(\rho). \end{aligned} \quad (9)$$

The appropriate numerical domain to solve Eq. (9) has the form of a cylinder of radius R_{box} and is apparently assumed to be of infinite height. The wave function is taken to be zero at the cylinder surface, which corresponds to artificially erecting the infinite potential barrier there. The boundary condition should also be adopted at the inner boundary $\rho = 0$. It is derived

by integrating Eq. (7) over an infinitesimally small region around the origin. This procedure treats the $l = 0$ states separately from the $l \neq 0$ states, and results into: (1) $d\psi/d\rho|_{\rho=0} = 0$ for $l = 0$ (the von Neumann boundary condition), and (2) $\psi(0) = 0$ for $l \neq 0$ (the Dirichlet boundary condition). When ψ is expanded in a series close to $\rho = 0$,

$$\begin{aligned}\psi(\rho) &= \psi(0) + \frac{1}{1!} \frac{d\psi}{d\rho} \Big|_{\rho=0} \rho + \frac{1}{2!} \frac{d^2\psi}{d\rho^2} \Big|_{\rho=0} \rho^2 + \dots \\ &= g_0 + g_1\rho + g_2\rho^2 + \dots,\end{aligned}\tag{10}$$

the continuity of the wave function indicates that all the derivatives $d^n\psi/d\rho^n$, $n \geq 1$, should be finite at $\rho = 0$. For $l = 0$, $d\psi/d\rho|_{\rho=0} = g_1 = 0$, i.e. the linear term is vanishing.

A direct approach to solve Eq. (9) is to discretize it by central differences. However, discretization of the term $(1/\rho)(d\psi/d\rho)$ makes the Hamiltonian a nonsymmetric matrix. In order to make it symmetric, Rizea et al. [28] proposed to replace ψ with

$$F(\rho) = \sqrt{\rho}\psi(\rho),\tag{11}$$

and to transform the Hamiltonian,

$$\tilde{H} = \frac{1}{\sqrt{\rho}}H\sqrt{\rho}.\tag{12}$$

Eqs. (11) and (12) keep the eigenstates orthonormal,

$$\int_0^{R_{box}} \psi_i^* \psi_j \rho d\rho = \int_0^{R_{box}} F_i^* F_j d\rho = \delta_{ij}.\tag{13}$$

One may notice that the scalar product of different F functions is computed as in a rectilinear system (see Sec. 4.5 for a much thorough explanation of this property).

The transformed Hamiltonian \tilde{H} is Hermitian, as evident from

$$\begin{aligned}& - \frac{\hbar^2}{2} \left[\frac{d}{d\rho} \left(\frac{1}{m^*} \frac{dF(\rho)}{d\rho} \right) - \left(\frac{l^2 - 1/4}{m^* \rho^2} + \frac{1}{2\rho} \frac{d(1/m^*)}{d\rho} \right) F(\rho) \right] \\ & + V(\rho)F(\rho) = EF(\rho).\end{aligned}\tag{14}$$

We note that Eqs. (11) and (12) represent the Liouville transformation when they are applied to the Bessel differential equation. For a general case of confining potential and effective-mass variation Eq. (14) does not have the Sturm-Liouville form, yet the problematic term $(1/\rho)(d/d\rho)$ is removed from the modified Hamiltonian, thus Eqs. (11) and (12) could be referred to as the *Liouville-like (LL) transformation*.

To solve Eq. (14), the boundary conditions for F should be determined from the boundary conditions for ψ . The series expansion of F determined from Eqs. (10) and (11) is

$$F(\rho) = g_0\rho^{\frac{1}{2}} + g_1\rho^{\frac{3}{2}} + g_2\rho^{\frac{5}{2}} + \dots, \quad (15)$$

wherefrom it follows that the n -th order derivative of F with respect to ρ is

$$\frac{d^n F(\rho)}{d\rho^n} = C_0(n)g_0\rho^{-n+\frac{1}{2}} + C_1(n)g_1\rho^{-n+\frac{3}{2}} + C_2(n)g_2\rho^{-n+\frac{5}{2}} + \dots. \quad (16)$$

Here, $C_i(n) = \prod_{q=0}^{n-1} (i + 1/2 - q)$. For $l \neq 0$, $g_0 = 0$ and the first and the second derivative of F are finite at $\rho = 0$. However, for $l = 0$ and at $\rho = 0$ the von Neumann boundary condition for ψ becomes the Dirichlet condition for F , i.e. $\lim_{\rho \rightarrow 0} F \sim \lim_{\rho \rightarrow 0} \sqrt{\rho} \rightarrow 0$ (see Eq. (15)). Since $g_0 \neq 0$, it follows from Eq. (16) that the derivatives of F diverge at $\rho = 0$, i.e. $\lim_{\rho \rightarrow 0} d^n F/d\rho^n \sim \lim_{\rho \rightarrow 0} \rho^{-n+1/2} \rightarrow \infty$. Thus it is difficult to compute the wave function ψ close to $\rho = 0$ by solving Eq. (14). Hence, the eigenenergies of the $l = 0$ states are determined with a large numerical error. In order to resolve this problem, Rizea et al. [28] used an asymmetric 3-point formula which fits the second derivative to an analytical solution. However, that approach generates nonsymmetric Hamiltonian matrices, and could therefore be impractical. We instead devise a scheme which constructs symmetric Hamiltonian matrices, and has the same accuracy as solving the original Schrödinger equation, which is elaborated in Sec. 4.5.

2.2. The discretization schemes

To solve both Eqs. (7) and (14), a grid with uniformly distributed points,

$$\rho_j = j\Delta\rho, \quad j = 0, 1, \dots, N_\rho, \quad (17)$$

is formed in the numerical domain $\rho \in [0, R_{box}]$ ($\Delta\rho$ is the step size). The difference equations are derived from Eqs. (7) and (14) by adopting the approximation of central differences for $j = 1, \dots, N_\rho - 1$.

(1) By applying the central differences to Eq.(7), we get

$$\begin{aligned}
S - FDM : \quad & - \frac{\hbar^2}{2(\Delta\rho)^2} \left[\frac{1 + \frac{1}{2j}}{m_{j+\frac{1}{2}}^*} \psi_{j+1} - \left(\frac{1 + \frac{1}{2j}}{m_{j+\frac{1}{2}}^*} \right. \right. \\
& + \left. \left. \frac{1 - \frac{1}{2j}}{m_{j-\frac{1}{2}}^*} + \frac{l^2}{j^2 m_j^*} \right) \psi_j + \frac{1 - \frac{1}{2j}}{m_{j-\frac{1}{2}}^*} \psi_{j-1} \right] \\
& + V_j \psi_j = E \psi_j, \tag{18}
\end{aligned}$$

which we call the *S-FDM* scheme, where the letter *S* symbolizes a direct solution of the Schrödinger equation. A careful inspection of this equation shows that the term proportional to the first derivative of ψ with respect to ρ makes the Hamiltonian matrix asymmetric.

(2) Similar to the *S-FDM* scheme, the central differences are also employed to discretize Eq. (14), which gives:

$$\begin{aligned}
LL - FDM : \quad & - \frac{\hbar^2}{2(\Delta\rho)^2} \left[\frac{1}{m_{j+\frac{1}{2}}^*} F_{j+1}^L - \left(\frac{1 + \frac{1}{2j}}{m_{j+\frac{1}{2}}^*} \right. \right. \\
& + \left. \left. \frac{1 - \frac{1}{2j}}{m_{j-\frac{1}{2}}^*} + \frac{l^2 - 1/4}{j^2 m_j^*} \right) F_j^L + \frac{1}{m_{j-\frac{1}{2}}^*} F_{j-1}^L \right] \\
& + V_j F_j^L = E F_j^L. \tag{19}
\end{aligned}$$

We refer to Eq. (19) as the *LL-FDM* scheme, and it is straightforward to show that the constructed Hamiltonian matrix is symmetric. But, as will be demonstrated below, the computation of the $l = 0$ states suffers from a low accuracy.

(3) In order to resolve the problems of the *S-FDM* and *LL-FDM* discretization schemes, we developed the third scheme. It replaces ψ_j in Eq. (18) with $F_j^{DL}/\sqrt{j\Delta\rho}$, and then multiplies the difference equation by $\sqrt{j\Delta\rho}$,

$$\begin{aligned}
DLL - FDM : \quad & - \frac{\hbar^2}{2\Delta\rho)^2} \left[\frac{1}{m_{j+\frac{1}{2}}^*} \frac{j + \frac{1}{2}}{\sqrt{j(j+1)}} F_{j+1}^{DL} - \left(\frac{1 + \frac{1}{2j}}{m_{j+\frac{1}{2}}^*} \right. \right. \\
& + \left. \left. \frac{1 - \frac{1}{2j}}{m_{j-\frac{1}{2}}^*} + \frac{l^2}{j^2 m_j^*} \right) F_j^{DL} + \frac{1}{m_{j-\frac{1}{2}}^*} \frac{j - \frac{1}{2}}{\sqrt{j(j-1)}} F_{j-1}^{DL} \right] \\
& + V_j F_j^{DL} = E F_j^{DL}. \tag{20}
\end{aligned}$$

Because the discretization is done by adopting the *LL* transformation at the discrete points ψ_j , we name it the *DLL-FDM* scheme. Such constructed Hamiltonian matrix is symmetric, hence its diagonalization bring in all the real eigenvalues.

(4) *R-FDM*: Yet another scheme is proposed by Rizea et al. to solve the problem of a low accuracy of the *LL-FDM* scheme [28]. It adapted the solution for an arbitrary potential to the solution in an infinite rectangular potential well. We refer to this discretization scheme as the *R-FDM*.

2.3. The boundary conditions

In order to solve the derived difference equations, conditions which are adopted at the outer boundary are either $\psi_{N_\rho} = 0$ or $F_{N_\rho} = 0$. They are implemented by removing the column $j = N_\rho$ from the system. On the other hand, the values of ψ and F at the inner boundary are implemented by either adding an equation for $j = 0$, or modifying an equation for $j = 1$, as will be explained separately for each discretization scheme.

S-FDM: When $l \neq 0$ there is a singular term l^2/ρ^2 in the Schrödinger equation, and physically we have to take $\psi_0 = 0$ at $\rho = 0$. For this case, no equation should be added or modified in the system in Eq. (18). On the other hand, for $l = 0$ the boundary condition at the inner boundary can be adopted in two forms.

(1) *The extended boundary condition*. Let us consider how the radial part of the Laplacian acts on $\psi(\rho)$,

$$\Delta_\rho \psi(\rho) = \frac{d^2\psi(\rho)}{d\rho^2} + \frac{1}{\rho} \frac{d\psi(\rho)}{d\rho}. \quad (21)$$

The limiting value of Eq. (21) at $\rho \rightarrow 0$ could be found by applying the l'Hospital rule to the second term in this equation, which gives

$$\lim_{\rho \rightarrow 0} \Delta_\rho \psi(\rho) = \lim_{\rho \rightarrow 0} \frac{d^2\psi(\rho)}{d\rho^2} + \lim_{\rho \rightarrow 0} \frac{d\psi(\rho)/d\rho}{\rho} = 2 \lim_{\rho \rightarrow 0} \frac{d^2\psi(\rho)}{d\rho^2}. \quad (22)$$

For $l = 0$, this equation is replaced in Eq. (9), and is discretized by assuming $\psi_{-1} = \psi_1$ and $m_{-1/2} = m_{1/2}$. It leads to an additional equation for $j = 0$

[28],

$$-\frac{\hbar^2}{2} \left\{ \frac{2}{(\Delta\rho)^2} \left[\frac{\psi_1}{m_{\frac{1}{2}}^*} - \left(\frac{1}{m_{\frac{1}{2}}^*} + \frac{1}{m_{-\frac{1}{2}}^*} \right) \psi_0 + \overbrace{\frac{\psi_{-1}}{m_{-\frac{1}{2}}^*}}^{\frac{\psi_1}{m_{\frac{1}{2}}^*}} \right] \right\} + V_0\psi_0 = E\psi_0. \quad (23)$$

This boundary condition requires extending the ρ axis to a range where $\rho < 0$, hence we call it the extended boundary condition (hereafter abbreviated by *e*).

(2) *The restricted boundary condition.* The *e* boundary condition has a drawback that the ρ axis is artificially extended to a range where ρ is not defined. The much simpler condition,

$$\psi_0 = \psi_1, \quad (24)$$

respects the requirement $\rho \geq 0$, and is therefore called the restricted boundary condition (abbreviated by *r*). The application of this boundary condition makes the equation for $j = 0$ redundant, which reduces the order of the Hamiltonian matrix by unity.

For $l = 0$, application of the restricted boundary condition to Eq. (18) changes the equation for $j = 1$,

$$-\frac{\hbar^2}{4} \frac{3}{(\Delta\rho)^2 m_{\frac{3}{2}}^*} (\psi_2 - \psi_1) + V_0\psi_0 = E\psi_0, \quad (25)$$

whereas the equation for $j = 0$ is superficial and is not added to the system in Eq. (18). Hence, the matrices constructed by means of the *Sr* – *FDM* scheme for $l = 0$ and $l \neq 0$ are of equal order. On the other hand, the order of the Hamiltonian matrix discretized by the *Se* – *FDM* scheme for $l = 0$ is larger by unity with respect to the $l \neq 0$ case.

LL-FDM: The boundary condition for the function F which should be supplied to the *LL-FDM* difference equation is

$$F_0^L = 0, \quad (26)$$

irrespective of the value of l .

DLL-FDM: In the *DLL-FDM* scheme $F_0^{DL} = 0$ is substituted into Eq. (20), but only after the limiting value for $j = 1$ is found,

$$\begin{aligned}
\frac{-\hbar^2}{2(\Delta\rho)^2} \lim_{j \rightarrow 1} \left[\frac{1}{m_{j-\frac{1}{2}}^*} \frac{j-\frac{1}{2}}{\sqrt{j(j-1)}} F_{j-1}^{DL} \right] &= \frac{-\hbar^2 \sqrt{\Delta\rho}}{4m_{\frac{1}{2}}^* (\Delta\rho)^2} \lim_{j \rightarrow 1} \left[\frac{F_{j-1}^{DL}}{\sqrt{(j-1)\Delta\rho}} \right] \\
&= \frac{-\hbar^2 \sqrt{\Delta\rho}}{4m_{\frac{1}{2}}^* (\Delta\rho)^2} \psi_0 = \frac{-\hbar^2 \sqrt{\Delta\rho}}{4m_{\frac{1}{2}}^* (\Delta\rho)^2} \psi_1 \\
&= \frac{-\hbar^2 \sqrt{\Delta\rho}}{4m_{\frac{1}{2}}^* (\Delta\rho)^2} \frac{F_1^{DL}}{\sqrt{\Delta\rho}} = \frac{-\hbar^2}{4m_{\frac{1}{2}}^* (\Delta\rho)^2} F_1^{DL}. \tag{27}
\end{aligned}$$

Therefore, Eq. (20) is for $j = 1$ modified to,

$$-\frac{\hbar^2}{2} \frac{1}{(\Delta\rho)^2} \left[\frac{3}{2\sqrt{2}} \frac{1}{m_{\frac{3}{2}}^*} F_2^{DL} - \frac{3/2}{m_{\frac{3}{2}}^*} F_1^{DL} \right] + V_1 F_1^{DL} = E F_1^{DL}. \tag{28}$$

This boundary condition obviously only affects the diagonal terms in the matrix constructed from Eq. (20), and therefore the symmetry of the Hamiltonian matrix is preserved after the application of the boundary condition. Note that the condition $\psi_1 = \psi_0$ is adopted in Eq. (24), therefore the boundary condition implemented in the *DLL-FDM* scheme is equivalent to the one used in the *Sr-FDM* scheme to solve the Schrödinger equation.

3. The error analysis

The error analysis of the different FDM schemes could be able to explain differences between them. However, in order to simplify this analysis, we assume that the effective mass is constant.

S-FDM: The difference equation for the wave function ψ constructed from Eq. (18) for the case $m^* = \text{const}$ has the form:

$$-\frac{\hbar^2}{2m^*} \left[\frac{\psi_{j+1} - 2\psi_j + \psi_{j-1}}{(\Delta\rho)^2} + \frac{\psi_{j+1} - \psi_{j-1}}{2j(\Delta\rho)^2} - \frac{l^2}{j^2(\Delta\rho)^2} \right] + V_j \psi_j = E \psi_j. \tag{29}$$

The radial part of the Laplacian acting on $\psi(\rho)$ is discretized such that

$$\begin{aligned}
& \frac{\psi_{j+1} - 2\psi_j + \psi_{j-1}}{\Delta\rho^2} + \frac{\psi_{j+1} - \psi_{j-1}}{2j\Delta\rho^2} \\
&= \left[\frac{1}{\rho} \frac{d}{d\rho} \left(\rho \frac{d\psi}{d\rho} \right) \right]_j \\
&+ \frac{(\Delta\rho)^2}{12} \left\{ \frac{1}{\rho} \frac{d}{d\rho} \left[\rho \frac{d}{d\rho} \left(\frac{1}{\rho} \frac{d}{d\rho} \left(\rho \frac{d\psi}{d\rho} \right) \right) \right] \right\}_j + \dots \\
&= \left[\frac{1}{\rho} \frac{d}{d\rho} \left(\rho \frac{d\psi}{d\rho} \right) \right]_j + \vartheta(\Delta\rho^2). \tag{30}
\end{aligned}$$

Because the derivatives of $\psi(\rho)$ computed by means of the *S-FDM* are finite, the *S-FDM*'s order is $\vartheta(\Delta\rho^2)$.

LL-FDM: The *LL-FDM* equation for $F(\rho)$ derived from Eq. (19) is

$$-\frac{\hbar^2}{2m^*(\Delta\rho)^2} \left(F_{j+1}^L - 2F_j^L + F_{j-1}^L - \frac{l^2 - 1/4}{j^2} F_j^L \right) + V_j F_j^L = E F_j^L. \tag{31}$$

The error of the *LL-FDM* discretization scheme can be estimated by using [29]

$$\frac{F_{j+1}^L - 2F_j^L + F_{j-1}^L}{\Delta\rho^2} = \left(\frac{d^2 F}{d\rho^2} \right)_j + \frac{(\Delta\rho)^2}{12} \left(\frac{d^4 F}{d\rho^4} \right)_j + \frac{(\Delta\rho)^4}{360} \left(\frac{d^6 F}{d\rho^6} \right)_j + \dots \tag{32}$$

Because all the derivatives $d^n F/d\rho^n$ for $l \neq 0$ are finite in the whole domain, the second derivative is approximately given as

$$\left(\frac{d^2 F}{d\rho^2} \right)_j = \frac{F_{j+1}^L - 2F_j^L + F_{j-1}^L}{\Delta\rho^2} + \vartheta(\Delta\rho^2), \tag{33}$$

where $\vartheta(\Delta\rho^2)$ is the error estimate. For $l = 0$, all the derivatives of the function $F(\rho)$ are infinite at $\rho = 0$, which makes use of this discretization scheme inconvenient in practice.

For $\rho = \Delta\rho$, from Eq. (16) it follows

$$\left. \frac{d^4 F}{d\rho^4} \right|_{\rho=\Delta\rho} \approx C_0(4) \cdot g_0 \Delta\rho^{-\frac{7}{2}}. \tag{34}$$

Thus, the second derivative at the $j = 1$ point is approximated as

$$\left(\frac{d^2 F}{d\rho^2}\right)_{j=1} \approx \frac{F_2^L - 2F_1^L + F_0^L}{\Delta\rho^2} - \frac{C_0(4)}{12} \frac{F_1^L}{\Delta\rho^2} + \vartheta(\Delta\rho^2). \quad (35)$$

Hence, if the standard three-point discretization formula for the second derivative is used at the grid points near the origin, F is computed at $\Delta\rho$ with a much larger than $\vartheta(\Delta\rho^2)$.

DLL-FDM: Similar to the previous two discretization formulas, the difference equation for F according to the *DLL-FDM* scheme is simply obtained from Eq. (20),

$$\begin{aligned} & - \frac{\hbar^2}{2m^*(\Delta\rho)^2} \left[\frac{j + \frac{1}{2}}{\sqrt{j(j+1)}} F_{j+1}^{DL} - \left(2 + \frac{l^2}{j^2}\right) F_j^{DL} \right. \\ & \left. + \frac{j - \frac{1}{2}}{\sqrt{j(j-1)}} F_{j-1}^{DL} \right] + V_j F_j^{DL} = E F_j^{DL}. \end{aligned} \quad (36)$$

Because the transformation in Eq. (12) is applied to the difference equation after the boundary conditions are implemented, the error of the *DLL-FDM* discretization is of the same order as the error of the discretization by the *S-FDM* scheme. The eigenvalues obtained by means of the *DLL-FDM* and *Sr-FDM* schemes are in fact equal, because the *DLL-FDM* scheme is obtained by transformation of the *Sr-FDM* equations (Eqs. (18) and (24)).

The error of the *DLL-FDM* discretization is estimated from the error of the finite difference approximation for the Laplacian acting on $\psi = F/\sqrt{\rho}$ (see Eq. (29)). When it is multiplied by $\sqrt{j\Delta\rho}$, the error becomes of the order $\sqrt{j\Delta\rho} \cdot \vartheta(\Delta\rho^2)$. It thus ranges from $\vartheta(\Delta\rho^{2.5})$ at the grid points near the origin to $\vartheta(\Delta\rho^2)$ at the grid points close to the outer numerical boundary. Hence, the error of the *DLL-FDM* approximation is smaller at the grid points which are closer to the inner boundary. It thus indicates that the energy levels computed by means of the *DLL-FDM* are more accurate than those determined by the *LL-FDM* scheme, irrespective of the value of l .

4. The numerical results for quantum wire states

We will use the mentioned discretization schemes to compute the energy levels in quantum wires based on the GaAs and $\text{Al}_{0.3}\text{Ga}_{0.7}\text{As}$ materials,

for the following potentials: (i) the infinite rectangular potential well in a freestanding GaAs quantum wire (see Fig. 1(a)), (ii) the potential of the linear harmonic oscillator in a freestanding GaAs quantum wire, which is illustrated in Fig. 1(b), (iii) the confinement inside the core of the core-shell GaAs/Al_{0.3}Ga_{0.7}As quantum wire (type I-c quantum wire), which is shown in Fig. 1(c), and (iv) the potential which confines the electrons inside the shell of the core-shell Al_{0.3}Ga_{0.7}As/GaAs quantum wire (type I-s quantum wire), which is displayed in Fig. 1(d). The potential (a) is usually employed to model states in freestanding quantum wires, whereas the model (b) can be used to approximate potentials in freestanding quantum wires which arise from the self-consistency effects. The models (c) and (d) are employed for computations of the states in core-shell quantum wires, and assume confinement in the core and shell, respectively. The effective-mass Schrödinger equation can be analytically solved for all these cases, thus the exact energy levels are known, and the accuracy of the proposed discretization schemes can be estimated for all four potentials. The parameters of the materials are taken from Ref. [30].

4.1. The infinite rectangular potential well in a free-standing quantum wire

Some quantum wires are formed as freestanding, either by etching [31, 32] or the VLS technique [33]. The electron in them is in fact confined by a few eV large band offset equal to the electron affinity. It is therefore localized almost fully inside the wire, as in an infinitely deep axially symmetric potential well. We assume that the potential inside the quantum wire equals zero and that it is infinite outside the wire,

$$V(\rho) = \begin{cases} 0, & \rho \leq R_w \\ \infty, & \rho > R_w \end{cases}. \quad (37)$$

The Schrödinger equation for this case has the form of the Bessel differential equation [29], whose solutions are

$$E_{l,n} = \frac{\hbar^2(\alpha_{l,n})^2}{2m^*R_w^2}, \quad (38)$$

and

$$\psi_{l,n}(\rho) = \frac{\sqrt{2}}{R_w} \frac{J_l(\alpha_{l,n}\rho/R_w)}{|J_{l+1}(\alpha_{l,n})|},$$

where $\alpha_{l,n}$ is the n th zero of the Bessel function of the first kind $J_l(x)$.

The computed wave functions for $l = 0$ and $n=1, 2,$ and 3 are shown in Fig. 2. The dashed lines and the lines denoted by symbols show the results of the *LL-FDM* and *DLL-FDM* discretizations, respectively, which are compared with the analytical solutions, displayed by solid lines. The wave functions determined by the *DLL-FDM* scheme obviously nicely fits the analytical solutions. On the other hand, the wavefunctions which are computed by means of the *LL-FDM* exhibit a substantial difference from the analytical solutions, especially at $\rho \ll R_w$. As we previously inferred from Eq. (35), the approximation of the second derivative, given by Eq. (33), is not valid at the grid points near the origin. Therefore, the *LL-FDM* fails to properly reproduce the wave function close to $\rho = 0$. Nonetheless, as Fig. 2 shows the wave functions of larger n determined by the *LL-FDM* differ less from the exact result. It is a consequence of the increasing number of oscillations in higher-energy states, which effectively narrows the region near the origin where $|\psi|$ is large and where the *LL-FDM* discretized function F is computed with a large error. Notice that the value of ψ at $\rho = 0$ could not be retrieved from our *LL-FDM* calculation, since $F(\rho)/\sqrt{\rho}$ is indeterminate at $\rho = 0$.

The *LL-FDM* and *DLL-FDM* schemes are also compared in Fig. 3, where variation of the relative errors of the energy levels with the number of grid points is shown. It is evident from Figs. 3(a) and 3(b) that the relative error $\delta E = \Delta E/E_{analytical}$ ($\Delta E = |E - E_{analytical}|$ is the absolute error) of the energy levels computed by means of the *DLL-FDM* is an order of magnitude smaller than the relative error of the *LL-FDM* discretization. Also, the two discretization schemes differ in the dependence of δE on the level number n . For a given N_{grid} , δE determined by means of the *DLL-FDM* increases with n . It is a consequence of the increasing frequency of the wave function oscillations when n increases, which are difficult to accurately model with a small number of grid points. Therefore, the relative error for higher states is large when N_{grid} is small. On the other hand, the relative errors of the energy levels computed by means of the *LL-FDM* decrease when n increases, which is associated with the demonstrated narrowing of the region where the deviation of ψ from the accurate wave function is large (see Fig. 2). Furthermore, as *a priori* expected, the relative errors of the energy levels shown in both Figs. 3(a) and (b) decay when the number of grid points increases. We include in Fig. 3(c) the relative error of the energy levels determined by the *R-FDM* scheme. The error of the *R-FDM* scheme is

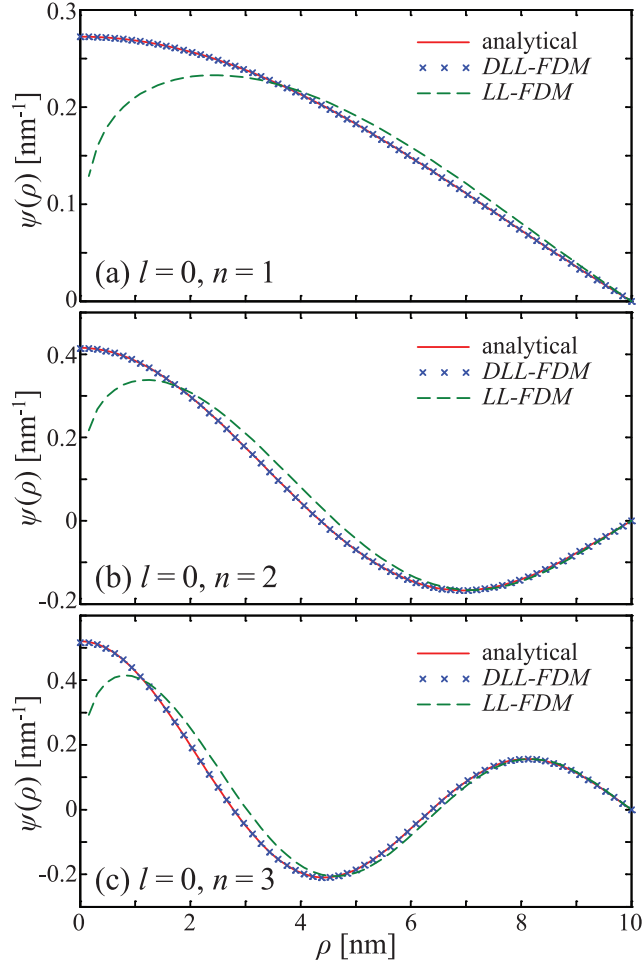


Figure 2: The radial parts of the wave functions calculated with the *DLL-FDM* scheme (blue symbols), the *LL-FDM* scheme (dashed green lines), and analytical wave functions (solid red lines) for $l = 0$: (a) the ground ($n = 1$) state, (b) the $n = 2$ state, and (c) the $n = 3$ state. Here $N_{grid} = 64$.

definitely lower than of the other two for $n = 1$, because the wavefunction is conveniently fitted by a polynomial $P(\rho)$ of some degree [28]. However, the use of the R - FDM scheme is limited for higher energy states, because they are more oscillatory. Then in order to improve the accuracy of the R - FDM scheme, it is necessary to increase the order of the polynomial which is used for the fitting procedure, which was however not proposed in Ref. [28].

For $l \neq 0$ the approximation of the second derivative by the LL - FDM discretization given by Eq. (33) gives results for the energy levels which are comparable to the DLL - FDM . Nevertheless, the error of the DLL - FDM approximation is smaller than the error of the LL - FDM , due to a much better description of the wave function at the grid points close to $\rho = 0$. It is indeed demonstrated in Fig. 4, where the absolute errors of the $n = 1, 2$, and 3 energy levels are shown as function of N_{grid} for $l = 1$. Here, not so large difference between the results obtained by the two methods is observed as in Fig. 3 for the $l = 0$ state. This is mainly because the Dirichlet boundary condition for ψ at the inner boundary is accurately reproduced by both the LL - FDM and the DLL - FDM when $l = 1$. Nonetheless, as the error analysis of the two approximations showed, the DLL - FDM delivers the energy states with a smaller absolute error than the LL - FDM scheme. As apparent from Fig. 4, the errors of the $l \neq 0$ energy levels determined by both discretization schemes increase with the level number, opposite to what was previously shown in Fig. 3(b) for the $l = 0$ states found by the LL - FDM . Dotted lines in Fig. 4 display the results of the R - FDM calculation for the $l = 1$ energy levels. Similar to the $l = 0$ case shown in Fig. 3, a smaller error is obtained for the $n = 1$ state, but the error of computation of the $n > 2$ states by the R - FDM is larger than of both the DLL - FDM and LL - FDM schemes.

Finally, we compare in Fig. 5 the errors of the $l = 0$ states computed by the $Se - FDM$ and $Sr - FDM$ schemes. For all the values of n , the absolute errors decay nearly exponentially with the number of grid points. However, the $Sr - FDM$ scheme delivers a few times smaller error than the $Se - FDM$, which could be explained as follows. The slope at $\rho = 0$ is nonzero in the $Se - FDM$ scheme, which increases the eigenenergy with respect to the value determined by the $Sr - FDM$ scheme. The error is smallest for the ground state, as displayed in Fig. 5(a), whereas the higher states are more oscillatory, and the errors of their energies, shown in Figs. 5(b) and (c) for $n = 2$ and $n = 3$, are much larger than for the $n = 1$ state. Nonetheless, in all the displayed cases in Fig. 5 the errors of the energy levels continuously decrease with N_{grid} . As a matter of fact, the slopes of the $Se - FDM$ wave functions

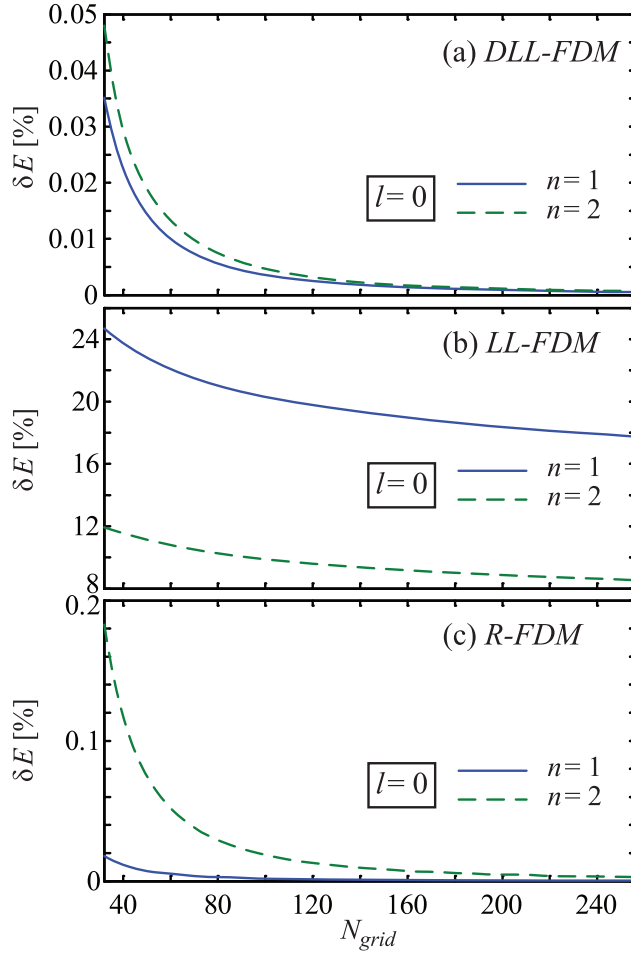


Figure 3: The relative errors of the $l = 0$ energy levels, as function of the number of grid points for: (a) the *DLL-FDM*, (b) *LL-FDM*, and (c) *R-FDM*. δE is shown for the ground $n = 1$ state (solid blue lines) and the $n = 2$ state (dashed green lines).

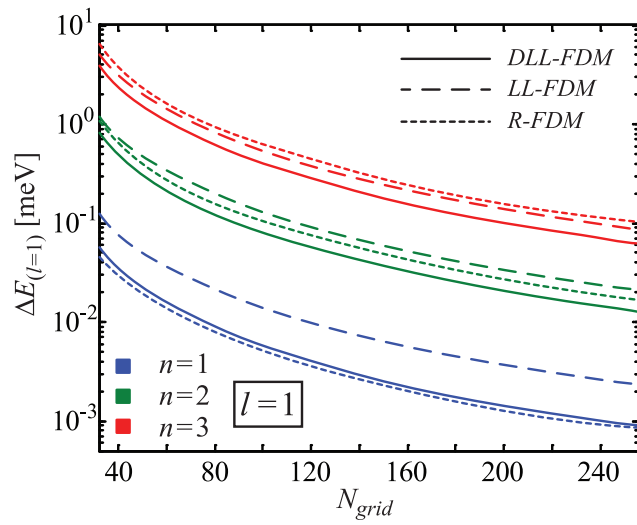


Figure 4: The absolute errors of the $n = 1$ (blue lines), $n = 2$ (green lines), and $n = 3$ (red lines) states of the orbital quantum number $l = 1$ in the rectangular infinite potential well in the freestanding quantum wire as function of the number of grid points. The *DLL-FDM* (solid lines), the *LL-FDM* (dashed lines) and the *R-FDM* (dotted lines) schemes are compared.

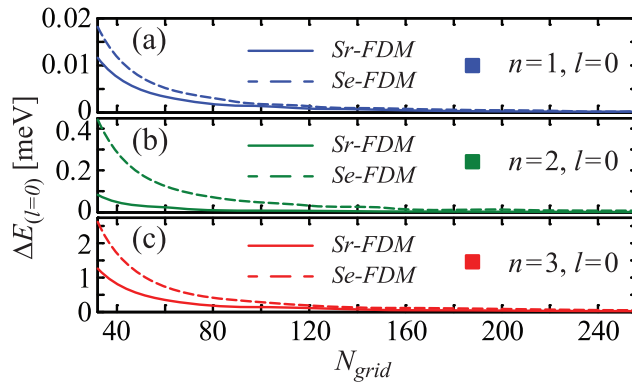


Figure 5: Variation of the absolute errors of the three lowest $l = 0$ energy levels for the infinite rectangular potential in a freestanding quantum wire with the number of grid points for: (a) the ground $n = 1$ state, (b) the $n = 2$ state, and (c) the $n = 3$ state. Solid lines are for the $S_r - FDM$ discretization, whereas dashed lines are the results of the $S_e - FDM$ calculation.

at the origin tend to zero when the grid size increases. It accounts for the convergence of the $S_r - FDM$ and $S_e - FDM$ results to each other when N_{grid} increase, as shown in each panel of Fig. 5.

4.2. The potential of a linear harmonic oscillator in a free-standing quantum wire

The confining potentials of the particles in a quantum wire are usually assumed to be constant in each material, but vary abruptly due to band offsets at interfaces between different materials. The external fields [16], mechanical strain [34], interdiffusion [35], and self-consistency effects [15, 31] may change such potential profiles. Self-consistency effects are known to lead to potentials which may be approximated by parabolas [31, 36]. Moreover, a linear harmonic oscillator is an extremely useful model in quantum mechanics.

In the analyzed axially symmetric quantum wire, the model of an isotropic 2D linear harmonic oscillator is adopted.

$$V(\rho) = m\omega^2\rho^2/2, \quad (39)$$

for which there exist analytical solutions for the eigenenergies, given by

$$E_{l,n} = \hbar\omega(2n + l + 1), \quad (40)$$

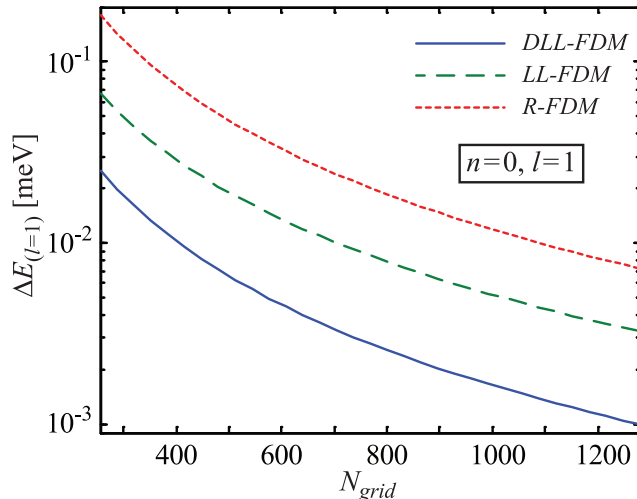


Figure 6: The absolute errors of the $(n = 1, l = 1)$ energy level in the 2D quantum harmonic oscillator computed by the *DLL-FDM* (solid line), the *LL-FDM* (long dashed line), and the *R-FDM* (short dashed line) scheme as function of the number of grid points.

where n denotes the principal quantum number, which is a nonnegative integer.

In Fig. 6 we compare the relative errors of the $(l = 1, n = 0)$ state for $\hbar\omega = 10$ meV, which are made by the *DLL-FDM* (solid lines), the *LL-FDM* (dashed lines), and the *R-FDM* (dotted lines) discretization schemes. The numerical boundary is positioned at $R_{box} = 100$ nm, which mimics experimental conditions in wide quantum wires formed by lithography and etching [31, 32] rather than in those made by the *VLS* technique. The choice of a wider wire here largely avoids the problem of reduced accuracy due to the cutoff of the parabolic potential at $\rho = R_{box}$. However, for the larger selected domain, to match the range of the step size in Figs. 2-5, it was necessary to form a larger grid. The case $l = 1$ is shown in Fig. 6 because it does not suffer from a low accuracy close to $\rho = 0$ as in the $l = 0$ case. Furthermore, the errors of the higher energy levels are larger than for the lowest energy state. It is because higher states extend spatially in larger regions, and therefore are affected more by the inaccuracy of the wave function close to the numerical boundaries. Hence, we display in Fig. 6 the energy of only the $n = 0$ state.

Fig. 6 shows that out of the three schemes the *DLL-FDM* approach de-

livers the most accurate energy levels. The energy levels determined by the *R-FDM* substantially deviate from the results of the *DLL-FDM* calculations. As a matter of fact, the error of the *R-FDM* scheme is an order of magnitude larger than the error of the *DLL-FDM*. Moreover, the *R-FDM* gives even less accurate results than the *LL-FDM*, which is a consequence of the adaptation in the *R-FDM* to the case when ψ can be approximated by a polynomial $P(\rho)$, as for the infinite rectangular potential barrier. Hence, the results of our calculations indicate that the *R-FDM* scheme is inaccurate when used to model the LHO quantum states.

4.3. The type-Ic confinement potential in a core-shell quantum wires

The third interesting case is a stepwise confinement potential varying along ρ ,

$$V(\rho) = \begin{cases} V_c, & \rho \leq R_c \\ V_s, & R_c < \rho < R_s \\ \infty, & \rho \geq R_s \end{cases} \quad (41)$$

It models core-shell quantum wires, where the core ($\rho \leq R_c$) and the shell ($R_c < \rho < R_s$) are made of different semiconductors. The effective mass values inside the core and the shell are different and are equal to $m = m_c$ and $m = m_s$, respectively, whereas V_c and V_s are the conduction band edges in the core and shell, respectively. Here, we assume that $V_c < V_s$, therefore the electron is confined in the core (type-Ic confinement). The band offset is defined by $V_{off} = V_s - V_c$. The analytical solution of the Schrödinger equation in the core is proportional to the Bessel function of the first kind $J_l(k\rho)$, and inside the shell it is a linear combination of the modified Bessel functions of the first and the second kind, $I_l(\kappa\rho)$ and $K_l(\kappa\rho)$, respectively. Here, $k = \sqrt{2m_c E/\hbar^2}$ and $\kappa = \sqrt{2m_s(V_{off} - E)/\hbar^2}$. Using the boundary conditions, $\psi(R_c^-) = \psi(R_c^+)$, $(1/m_c)\psi'(R_c^-) = (1/m_s)\psi'(R_c^+)$, and $\psi(R_s^-) = 0$ results into

$$\begin{vmatrix} J_l(kR_c) & -I_l(\kappa R_c) & -K_l(\kappa R_c) \\ \frac{k}{m_c} J_l'(kR_c) & -\frac{\kappa}{m_s} I_l'(\kappa R_c) & -\frac{\kappa}{m_s} K_l'(\kappa R_c) \\ 0 & I_l(\kappa R_s) & K_l(\kappa R_s) \end{vmatrix} = 0, \quad (42)$$

wherefrom the eigenenergies are computed. Here, the prime symbol denotes the first derivative with respect to either $k\rho$ or $\kappa\rho$.

To adjust the grid step to the previously analyzed potentials, the number of grid points is twice as large as in the case of the infinite well. The analyzed

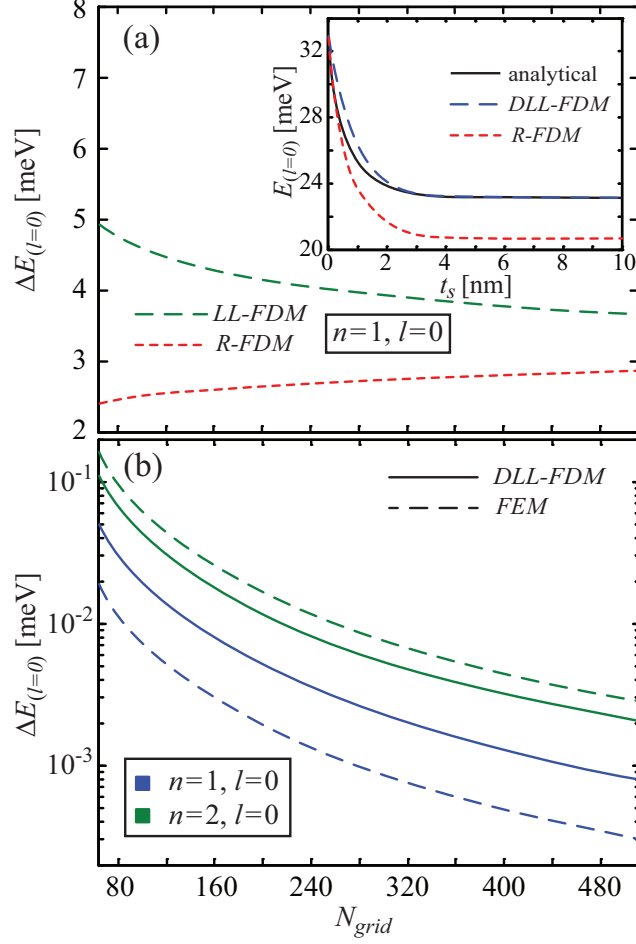


Figure 7: (a) Variation of the absolute errors of the ground state $l = 0$ eigenenergy for the type-Ic confinement potential in the core-shell quantum wire computed by the *LL-FDM* (green dashed lines) and *R-FDM* (dotted red lines) schemes with the number of grid points. Inset shows variation of the ground state eigenenergy with the shell thickness. (b) The absolute errors of the *DLL-FDM* (solid lines) and the *FEM* (dashed lines) calculations of the $l = 0$ levels: $n = 1$ (blue lines) and $n = 2$ (green lines).

system is the GaAs/(Al,Ga)As core-shell nanowire, with the core radius $R_c = 10$ nm, and the outer radius of the shell is $R_s = 20$ nm. The absolute errors of the $l = 0$ eigenenergies are displayed in Fig. 7, where Fig. 7(a) compares the *LL-FDM* and *R-FDM* schemes, and Fig. 7(b) shows the comparison between the *DLL-FDM* scheme and the *FEM*. As for the previous three potentials, the accuracy of the *DLL-FDM* scheme is much better than the accuracy of the *LL-FDM* scheme (compare Figs. 7(a) and (b)). But, opposite to the LHO, the ground state energy computed by the *R-FDM* has a better accuracy than the *LL-FDM*. Yet, the error of the *R-FDM* eigenenergy is much larger than the *DLL-FDM* result. We recall that an estimation of the range where the second derivative is adapted to the solution of the infinite rectangular quantum well is needed in the *R-FDM* scheme [28]. When the confinement potential in core-shell quantum wires is of type-Ic, we found that the *R-FDM* scheme gives the best result when the adaptation is done in the whole core, which is the result displayed in Fig. 7(a).

We also analyzed how the energy levels vary when the shell thickness $t_s = R_s - R_c$ decreases, which is plotted in Fig. 7(a). Here, the number of grid points in the core is fixed to 100. Because the wave function is confined in a larger portion of the structure, the error of the *R-FDM* approximation decreases when t_s decreases, and therefore its result, shown by the short dashed curve in the inset of Fig. 7(a) approaches the two other curves at $t_s = 0$. The *DLL-FDM* computed energy, displayed by the long dashed curve, differ negligibly from the analytical solution when $t_s > 2$ nm, whereas for smaller t_s the difference between the two is larger. A large error of the *R-FDM* for large t_s can be explained by the fact that the solution in the shell is expressed as a linear combination of the Bessel functions K_l and I_l . Such a combination implies that a higher order polynomial $P(\rho)$ should be used in the *R-FDM* scheme.

Since the results obtained by means of the *DLL-FDM* are much more accurate than both the *LL-FDM* and *R-FDM*, in Fig. 7(b) we choose to compare the *DLL-FDM* with the *FEM* calculation which employs the linear Lagrange basis and uses the same uniform grid as the *DLL-FDM*. Fig. 7(b) shows the absolute errors of the two lowest $l = 0$ energy levels computed by the *DLL-FDM* (solid lines) and the *FEM* (dashed lines) as function of the number of grid points. The accuracy of the ground energy level computed by the *FEM* is a few times better than the accuracy of the *DLL-FDM*, even though the lowest order approximations are adopted in both calculations. Also, the ground energy level obtained by means of the *FEM* exhibits a

faster convergence toward the exact value than the *DLL-FDM*. Nonetheless, the accuracy of the *DLL-FDM* is slightly better for the $n = 2$ state.

4.4. The type-Is confinement potential in core-shell quantum wires

Let us now consider the case of the potential as in Eq.(41), but for $V_c > V_s$, which assumes that the electron is mainly confined in the shell (type-Is confinement). The analytical solution in the core is proportional to the modified Bessel function of the first $I_l(\kappa\rho)$, whereas in the shell it is formed as a linear combination of the Bessel functions of the first and the second kind, $J_l(k\rho)$ and $Y_l(k\rho)$, respectively. Here, $k = \sqrt{2m_s E/\hbar^2}$, $\kappa = \sqrt{2m_c(V_{off} - E)/\hbar^2}$ and $V_{off} = V_c - V_s$. By using the same boundary conditions as for the type-Ic confinement, we derive the equation:

$$\begin{vmatrix} I_l(\kappa R_c) & -J_l(k R_c) & -Y_l(k R_c) \\ \frac{\kappa}{m_c} I_l'(\kappa R_c) & -\frac{k}{m_s} J_l'(k R_c) & -\frac{k}{m_s} Y_l'(k R_c) \\ 0 & J_l(k R_s) & Y_l(k R_s) \end{vmatrix} = 0. \quad (43)$$

The energy levels determined from this equation are used as a reference for assessing the accuracy of the *FDM* schemes.

We analyzed the (Al,Ga)As/GaAs core-shell nanowire, whose core and shell radii are $R_c = 3$ nm and $R_s = 6$ nm, respectively. The smaller dimensions are selected here than for the case of the type-Is confinement because we found almost no difference between the results of the *LL-FDM*, the *DLL-FDM*, and the *R-FDM* schemes for $R_c = 10$ nm and $R_s = 20$ nm. This is a consequence of the decay of the wave function to a negligible value inside the core for such a large radius, where the *LL-FDM* was previously demonstrated to lack accuracy. Thus the error of both the wave functions and the energy levels computed by the *LL-FDM* approaches the results obtained by the other methods. For $R_c = 3$ nm and $R_s = 6$ nm, however, the *FDM* schemes exhibit considerable mutual discrepancy, as Fig. 8 shows. The most accurate result is again computed by the *DLL-FDM* scheme. The core is here rather thin such that the wave function does not vanish in the core center, and is proportional to the modified Bessel function of the first kind I_l , which has a different shape than J_l to which the *R-FDM* scheme is adapted. Therefore, a large discrepancy of the *R-FDM* energy level from the *DLL-FDM* result is found. However, the *R-FDM* scheme has a slightly better accuracy than the *LL-FDM* approach. Therefore, the three schemes displayed in Fig. 8 compare similarly as for the case of type-Ic confinement (compare Figs. 7 and 8).

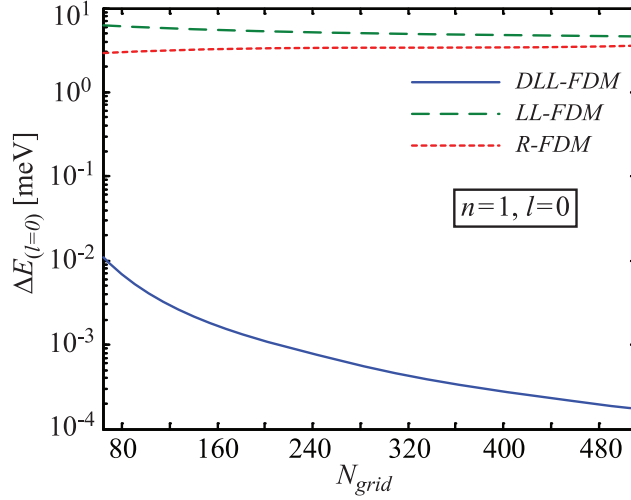


Figure 8: Variation of the absolute errors of the $l = 0$ ground state eigenenergy for the type-Is confinement in the core-shell quantum wire with the number of grid points determined by the *DLL-FDM* (solid blue lines), the *LL-FDM* (dashed green lines), and the *R-FDM* (dotted red lines).

4.5. A note on the PT symmetry of the Hamiltonian

From the analysis presented in previous sections we might recall that solving the original Schrödinger equation brings about a nonsymmetric Hamiltonian matrix. But, we found that all the eigenvalues of such a matrix are always real. More specifically, we found that the solutions of the equations according to the *Sr-FDM* and *DLL-FDM* schemes are equal, even though the Hamiltonian matrices which are constructed by the two schemes have different symmetry. At this point in our work, we raised the question about the reasons for the realness of the eigenvalues of the nonsymmetric Hamiltonian matrix. It needed examining the solutions of Eq. (7) more closely. In order to explain our findings, we rewrite Eq. (7) by changing the symbol ρ to x ,

$$\begin{aligned}
 & - \frac{\hbar^2}{2} \left[\frac{1}{m^*} \frac{d^2 \psi_x(x)}{dx^2} + \frac{1}{m^* x} \frac{d \psi_x(x)}{dx} + \frac{d}{dx} \left(\frac{1}{m^*} \right) \frac{d \psi_x(x)}{dx} - \frac{l^2 \psi_x(x)}{m^* x^2} \right] \\
 & + V(x) \psi_x(x) = E \psi_x(x).
 \end{aligned} \tag{44}$$

It is the Schrödinger equation for ψ_x ,

$$H_x \psi_x(x) = E \psi_x(x). \tag{45}$$

This equation is easily solved even if x is assumed to be a Cartesian coordinate. However, the Hamiltonian H_x is manifestly non-Hermitian,

$$\int_0^{R_{box}} \psi_{xi}^*(x) H_x \psi_{xj}(x) dx \neq \left[\int_0^{R_{box}} \psi_{xj}^*(x) H_x \psi_{xi}(x) dx \right]^*, \quad (46)$$

and hence the matrix representation of H_x is non-Hermitian as well. In the special case of real ψ_{xi} and ψ_{xj} the last equation points out that the Hamiltonian matrix would be nonsymmetric. Such a result was previously obtained by either the *Sr-FDM* or the *Se-FDM* discretization schemes.

Because the Hamiltonian H_x is non-Hermitian, it may *a priori* turn out that the eigenvalues are non-real. However, H_x satisfies another condition, which guarantees that all its eigenvalues are real. In order to formulate it, the range of x should be extended to $x < 0$. Also, because the wave functions should satisfy either the Dirichlet or the von Neumann boundary condition, $V(x)$ and $1/m^*(x)$ should be symmetric in the extended range of x : $V(-x) = V(x)$ and $1/m^*(-x) = 1/m^*(x)$. It is then straightforward to show that H_x commutes with the product of the space reflection operator \mathcal{P} and the time-reversal operator \mathcal{T} [37],

$$[H_x, \mathcal{PT}] = 0. \quad (47)$$

Since H_x satisfies Eq. (47) it is a \mathcal{PT} symmetric Hamiltonian [37].

If the same boundary conditions are imposed to both Eqs. (9) and (44), they should have the same spectrum (eigenvalues), despite the fact that H is a Hermitian operator, whereas H_x is not. Therefore, H_x is a non-Hermitian operator having real eigenvalues, which is a property of any \mathcal{PT} symmetric Hamiltonian. This conclusion is quite general and does not have any relation to how the Schrödinger equation is solved. It indicates that any method for solving the Schrödinger equation which (mistakenly or deliberately) treats ρ as a coordinate of the rectilinear system should deliver real eigenvalues. Hence, if multiplication by ρ is missing in the matrix elements of H , i.e. if they are computed as $\int \psi_i(\rho) H \psi_j(\rho) d\rho$, the same eigenvalues are obtained as if the matrix elements are properly computed as $\int \psi_i(\rho) H \psi_j(\rho) \rho d\rho$. But the boundary conditions must also be equal for these two calculations to give the same energy spectrum.

Let us refer back to our comparison of the different *FDM* schemes. The

LL transformed Hamiltonian \tilde{H} in Eq. (12) is Hermitian, such that it satisfies,

$$\int_0^{R_{box}} F_i^*(\rho) \tilde{H} F_j(\rho) d\rho = \int_0^{R_{box}} F_j^*(\rho) \tilde{H} F_i(\rho) d\rho, \quad (48)$$

therefore after the LL transformation, ρ is treated as a Cartesian coordinate. However, Eq. (14) is solved by applying a different boundary condition than for Eq. (9). It makes the results of the LL - FDM calculations different from those obtained by means of the S - FDM schemes. On the other hand, the DLL - FDM scheme produces a symmetric Hamiltonian matrix and gives the same energy levels as the Sr - FDM scheme. It is because equivalent boundary conditions are implemented in the two methods. Also, the Hamiltonian obtained by the adaptive calculation of Rizea et al. [28] is \mathcal{PT} symmetric. It explains why this procedure delivers all real eigenvalues even though the constructed Hamiltonian matrices are nonsymmetric.

The conclusions about the energy spectrum that have just been derived from the \mathcal{PT} symmetry property of the Hamiltonian H are quite general and are therefore not related to a specific numerical method for solving the effective-mass Schrödinger equation. Hence, they are valid for computations by the finite-element method and the method of expansion, for example. However, among all the methods, those which produce symmetric Hamiltonian matrices offer much more efficient numerical solutions of the eigenproblem due to the important advantages of symmetric matrices: abundance of software for their numerical diagonalization, generally faster diagonalization procedures, and reduced requirements for memory storage. Nonetheless, for a successful application of any such a method it is important to properly implement the boundary conditions, as is done by the DLL - FDM scheme.

5. Conclusions

An efficient discretization scheme to solve the Schrödinger equation in cylindrical coordinates is devised, and applied to compute the energy levels for a few potentials in axially symmetric quantum wires and quantum dots. It is constructed by the FDM discretization of the original Schrödinger equation, and the subsequent transformation applied to the difference equation. Thus the Hamiltonian matrix is symmetrized in discrete space. The scheme is demonstrated to lead to an improved accuracy of the numerical solution

close to the inner boundary of the numerical domain. Also, the Hamiltonian matrices which are constructed by the scheme are symmetric, and are therefore more efficiently diagonalized than the nonsymmetric matrices formed by a direct application of central differences to the Schrödinger equation. We infer that the proposed discretization scheme could be applied to other differential equations in cylindrical coordinates which contain the ρ -dependent part of the Laplacian. In addition to the symmetry of the Hamiltonian the scheme is shown to have an improved accuracy with respect to other methods close to $\rho = 0$. Moreover, it is shown to compare favorably well with the results of the finite-element calculations. The coincidence of the results obtained by some *FDM* schemes is explained by the \mathcal{PT} symmetry of the Hamiltonian, and the large error of some of them is found to be mainly a consequence of the peculiar boundary conditions.

6. Acknowledgements

This work was supported by the Ministry of Education, Science, and Technological Development of Serbia (project III 45003) and the Fonds Wetenschappelijk Onderzoek (Belgium).

References

- [1] R. Wagner and W. Ellis, *Appl. Phys. Lett.* 4 (1964) 89-90.
- [2] X. Duan, J. Wang, and C. M. Lieber, *Appl. Phys. Lett.* 76 (2000) 1116-1118.
- [3] D. Lucot, F. Jabeen, J.-C. Harmand, G. Patriarche, R. Giraud, G. Faini, and D. Maily, *Appl. Phys. Lett.* 98 (2011) 142114 (1-3).
- [4] D.C. Dillen, K. Kim, E.-S. Liu, and E. Tutuc, *Nature Nanotechnol.* 9 (2014) 116-120.
- [5] M.S. Gudiksen, L.J. Lauhon, J. Wang, D.C. Smith, and C.M. Lieber, *Nature (London)* 415 (2002) 617-620.
- [6] C. Cheng and H.J. Fan, *Nano Today* 7 (2012) 327-343.
- [7] V. Schmidt, J.V. Wittemann, S. Senz, and U. Gösele, *Adv. Mat.* 21 (2009) 2681-2702.

- [8] Y. Wu and P. Yang, *J. Am. Chem. Soc.* 123 (2001) 3165-3166.
- [9] T. Cohen-Karni, D. Casanova, J. Cahoon, Q. Qing, D. Bell, and C.M. Lieber, *Nano Lett.* 12 (2012) 2639-2644.
- [10] S.-K. Kim, R.W. Day, J.F. Cahoon, T.J. Kempa, K.-D. Song, H.-G. Park and C.M. Lieber, *Nano Lett.* 12 (2012) 4971-4976.
- [11] M. Tchernycheva, P. Lavenus, H. Zhang, A.V. Babichev, G. Jacopin, M. Shahmohammadi, F.H. Julien, R. Ciecchonski, G. Vescovi, and O. Kryliouk, *Nano Lett.* 14 (2014) 2456-2465.
- [12] C.K. Chan, H. Peng, G. Liu, K. McIlwrath, X.F. Zhang, and R.A. Huggins, and Y. Cui, *Nature Nanotechnol.* 3 (2008) 31-35.
- [13] P. Xie, Q. Xiong, Y. Fang, Q. Qing, and C.M. Lieber, *Nature Nanotechnol.* 7 (2012) 119-125.
- [14] H. Peelaers, B. Partoens, and F.M. Peeters, *Phys. Rev. B* 82 (2010) 113411.
- [15] M. Tadić and Z. Ikonić, *Phys. Rev. B* 50 (1994) 7680-7688.
- [16] Y. Sidor, B. Partoens, and F. M. Peeters, *Phys. Rev. B* 71 (2005) 165323.
- [17] M.-E. Pistol, C.E. Pryor, *Phys. Rev. B* 78 (2008) 115319.
- [18] V.V.R. Kishore, N. Čukarić, B. Partoens, M. Tadić, and F.M. Peeters, *J. Phys. Cond. Mat.* 24 (2012) 135302.
- [19] H. Taşeli, and A. Zafer, *Int. J. Quant. Chem.* 61 (1997) 759-768.
- [20] N. Čukarić, V. Arsoški, M. Tadić, and F. M. Peeters, *Phys. Rev. B* 85 (2012) 235425 (1-11).
- [21] C. Galeriu, L.C.L.Y. Voon, R. Melnik, M. Willatzen, *Comp. Phys. Comm.* 157 (2004) 147-159.
- [22] K.W. Morton, *Comp. Phys. Comm.* 12 (1976) 99-108.
- [23] J.W. Thomas, *Numerical Partial Differential Equations: Finite Difference Methods - Volume 1*, Springer-Verlag, New York, p. 1-435, 1995.

- [24] V. A. Schweigert, and F. M. Peeters, Phys. Rev. B 60 (1999) 3084-3087.
- [25] S. Zhao, Comp. Meth. Appl. Mech. Eng. 196 (2007) 5031-5046.
- [26] I. S. Ibrahim, V. A. Schweigert, and F. M. Peeters, Phys. Rev. B 57 (1998) 15416-15427.
- [27] O. Stier, Electronic and Optical Properties of Quantum Dots and Wires, Wissenschaft&Technik Verlag, Berlin, 2001.
- [28] M. Rizea, V. Ledoux, M. Van Daele, G. Vanden Berghe, N. Carjan, Comp. Phys. Comm. 179 (2008) 466-478.
- [29] M. Abramowitz, I.A. Stegun, Handbook of Mathematical Functions with Formulas, Graphs, and Mathematical Tables, 10th ed., Dover, New York, 1972.
- [30] J. Singh, Physics of Semiconductors and Their Heterostructures, Mc Graw Hill, New York, 1993.
- [31] C.R. Proetto, Phys. Rev. B 45 (1992) 11911-11917.
- [32] C. Youtsey, R. Grundbacher, R. Panepucci, I. Adesida, and C. Caneau, J. Vac. Sci. Technol. B 12 (1994) 3317-3321.
- [33] J.F. Wang, M.S. Gudiksen, X.F. Duan, Y. Chi, C.M. Lieber, Science 293 (2001) 1455-1457.
- [34] V. Arsoski, M. Tadić, and F. M. Peeters, Phys. Rev. B 87 (2013) 085314 (1-14).
- [35] O. Gunawan, H. S. Djie, and B. S. Ooi, Phys. Rev. B 71 (2005) 205319 (1-10).
- [36] F.M. Peeters, Phys. Rev. B 42 (1990) 1486-1487.
- [37] C.M. Bender, Rep. Prog. Phys. 70 (2007) 947-1018.